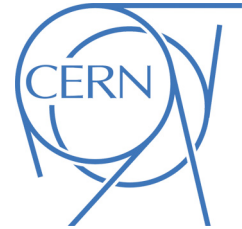# ATLAS NOTE

ATLAS-CONF-2012-047

May 18, 2012

Improved electron reconstruction in ATLAS using the Gaussian Sum Filter-based model for bremsstrahlung

The ATLAS Collaboration

Abstract

The behavior of high-energy electrons in the ATLAS Inner Detector is dominated by radiative energy losses (bremsstrahlung) as they traverse matter. These can be significant considering the substantial amount of material that the Inner Detector contains and can give rise to deviations from the original charged particle's path as it propagates through the magnetic field. As a result, significant inefficiencies, both during the electron trajectory reconstruction and in the determination of the corresponding track parameters in the bending plane, can be observed. In this note, we present a modification of the electron reconstruction in ATLAS that uses track refitting with the Gaussian Sum Filter (GSF) algorithm, with the aim of improving the estimated electron track parameters. The performance of this new scheme is compared to that of the existing standard electron reconstruction, for electron transverse energies between 7 GeV and 80 GeV.

1   Introduction

An electron can lose a significant amount of its initial energy due to bremsstrahlung energy losses when interacting with the material it traverses. This is particularly relevant with modern tracking detector designs, based on semiconductor technologies developed for optimal performance in stringent environments such as those at the LHC. Such tracking detectors are characterized by non-uniformly distributed material with high concentrations at specific radial positions. While the detector elements themselves contribute very little to the overall material budget, the requirements for on-detector electronics, power distribution, cooling and mechanical support add significantly to it. Because of the electron's small mass, radiative losses can be substantial, resulting in alterations of the curvature of the electron's trajectory when it propagates through a magnetic field and hence of the electron track.

The ATLAS [1] Inner Detector allows the measurement of the trajectories of charged particles over five units in pseudorapidity, $|\eta| < 2.5$, as well as the determination of their production vertices. It comprises three sub-systems: a silicon Pixel Detector at low radius providing three space points per track, a Semiconductor Tracker (SCT) providing four measurements in two stereo coordinates and a Transition Radiation Tracker (TRT) providing track-following and electron identification capability up to $|\eta| = 2.0$. The whole tracker is surrounded by a solenoidal magnet with a central field of 2 T. The overall material distribution of the ATLAS Inner Detector is shown in Fig. 1, illustrating significant increases at higher pseudorapidities.

The electron reconstruction scheme used for the 2010 and 2011 publications of ATLAS results employs the same tracking algorithm for all charged particles, with all tracks fitted using a pion particle hypothesis to estimate the material effects. The lack of special treatment for bremsstrahlung effects results in inefficiencies in reconstructing the electron trajectory. It also results in the degradation of the estimated track parameters, increasing with the amount of material encountered. This has a strong dependence on the electron pseudorapidity. By taking into account bremsstrahlung losses (and the resulting alteration of the track curvature) by using the Gaussian Sum Filter (GSF) [2, 3] approach, the estimated electron track parameters are expected to be improved.
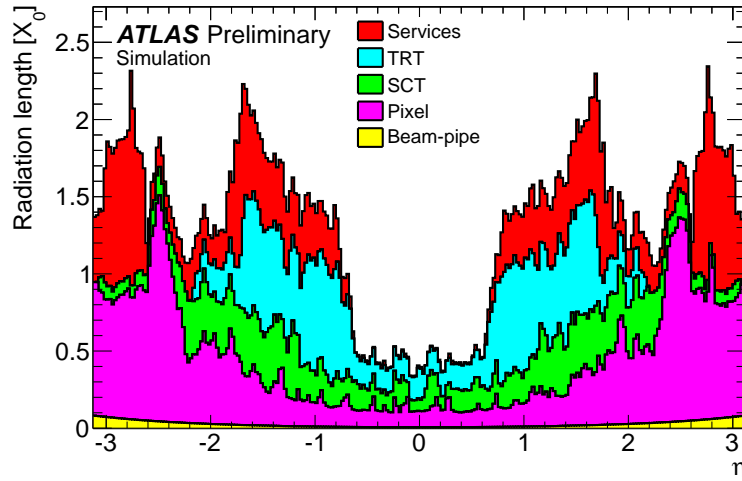

Figure 1: *Distribution of the Inner Detector material thickness given separately for each sub-detector as a function of the pseudorapidity η reflecting the Inner Detector description implemented in the current ATLAS simulation. The material of the Pixel and SCT detectors include the passive material mostly located behind the active silicon sensors. The track-refitting technique presented in this note has been developed primarily to account for the radiative energy losses due to this material.*

A two-step programme is underway in ATLAS to improve electron reconstruction: first to correct all track parameters associated to electron candidates by performing bremsstrahlung *refitting* prior to electron reconstruction and identification, and eventually to perform bremsstrahlung *recovery* at the initial step of the electron trajectory formation to allow for more efficient track reconstruction. Correcting for bremsstrahlung effects will also mean that track-to-calorimeter matching will use a better defined track, the electron four-momentum vector will be better determined and particle identification tools will benefit from those improvements. Such a procedure would eventually allow for more optimal electron identification in analyses, thereby potentially recovering significant efficiency losses, especially at low transverse momentum.

This note describes the results of the first step, namely applying, prior to electron reconstruction and identification, a bremsstrahlung refit with the GSF algorithm to tracks already associated to electron candidates. The impact on the determination of track parameters and more global combined-parameters involving the calorimeter, will be presented. In Section 2, a brief overview of the Gaussian Sum Filter approach and the new electron reconstruction scheme are presented. The effects on the reconstructed track parameters are discussed in Section 3, and more global parameters involving the electromagnetic calorimeter are reviewed in Section 4. Finally, a specific example involving electrons with small transverse momenta is presented in Section 5.

2 Electron Reconstruction

Electron candidates are selected by matching reconstructed tracks to clusters formed by the energy deposited in the electromagnetic calorimeter [4, 5]. The reconstruction of a charged-particle track in AT-LAS involves determining the particle's trajectory in the tracker from the detector response and then estimating the track parameters that best describe it. The latter include two parameters that give the transverse (d_0) and the longitudinal position (z_0) of the perigee (impact parameters), two parameters that describe the direction of the charged particle at this point (ϕ, θ) and one parameter that provides the inverse track momentum multiplied by the charge (q/p). The errors on the track parameters originate from experimental uncertainties due to the intrinsic resolution of the tracker sensors and the interaction of the charged particle with the detector material. The track parameters and their corresponding uncertainties are estimated from the track-fitting process. For muons or pions (neglecting hadronic interactions), an essentially linear least-squares fit using a linearized helical model with scattering angle formulation [6, 7] is used to estimate the trajectory from the set of experimental measurements. Unfortunately in the case of electrons, such an assumption is not valid since their trajectory is affected by energy losses dominated by bremsstrahlung.

A well-known model of the energy loss of electrons due to bremsstrahlung was proposed by Bethe and Heitler [8]. According to this model, the probability density function for an electron to retain a portion $z = \frac{E_f}{E_i}$ of its initial energy E_i as its final energy E_f, is given by [2, 8]:

$$f(z) = \frac{[-\ln z]^{a-1}}{\Gamma(a)}, \quad \text{with} \quad a = t/\ln 2, \quad 0 < z < 1 \tag{1}$$

where t is the thickness of the material traversed by the electron in units of radiation length X_0. The expression above needs to be modified in order to account for processes, such as the Landau-Pomeranchuk-Migdal (LPM) or the Ter-Mikaelian effects, that become prominent at electron energies of the order of several GeV or higher [9]. The resulting probability density function cannot be expressed in an analytical form, but it can be implemented numerically in simulation engines like GEANT4 [10] providing the model that describes the radiative energy losses of electrons. Under those conditions, a non-linear fitter may provide better estimations of the track parameters. Such a fitter, based on a generalisation of the Kalman Filter [11], and called the Gaussian Sum Filter (GSF), has been developed in [3]. It assumes that
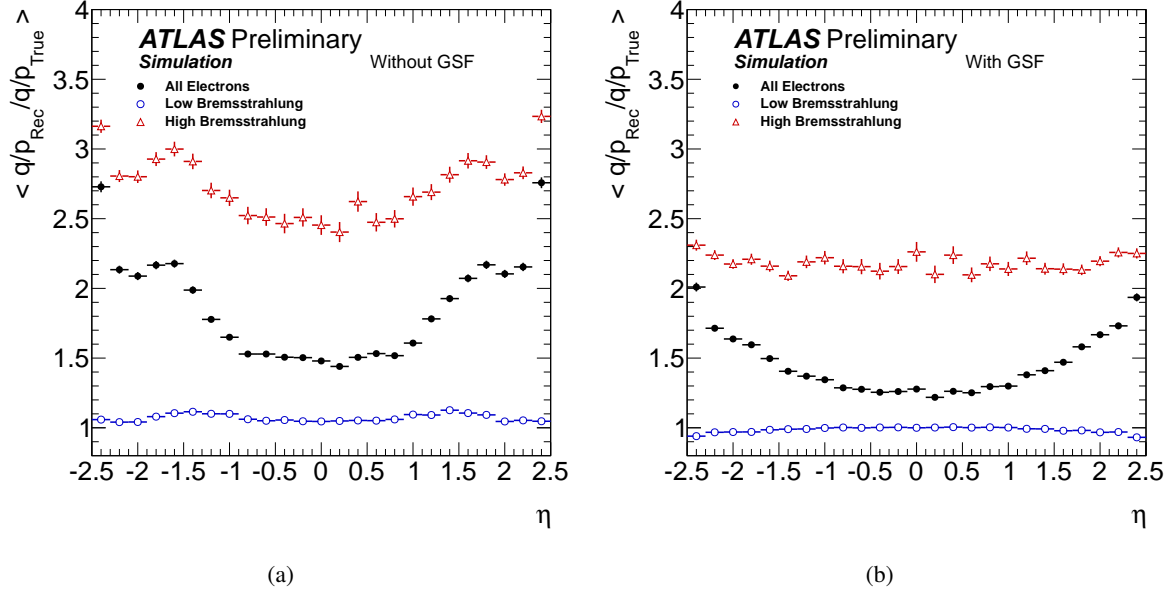
Figure 2: *Mean value of the ratio of the reconstructed over the true electron inverse momentum times charge (q/p) as a function of pseudorapidity for single electrons with transverse momentum between 7 and 80 GeV that lose less than (open points) and greater than (open triangles) 20% of their energy due to bremsstrahlung in the silicon detector and surrounding infrastructure without (a) and with (b) GSF refitting applied. Electrons that suffer significant bremsstrahlung losses dominate the high pseudorapidity regions. This explains the larger dependence with pseudorapidity when all the electrons are averaged (solid points).*

the trajectory state can be approximated as a weighted sum of Gaussian functions. The GSF splits the experimental noise into individual Gaussian components and uses the Kalman filter technique in order to process each one. The GSF therefore consists of a number of Kalman filters running in parallel, each one representing a different contribution to the full Bethe-Heitler spectrum. In its current ATLAS implementation, the Gaussian Sum Filter is used to account for the radiative loss effects of electrons as they traverse the silicon trackers. In the case of the Transition Radiation Tracker, it has been found that due to the more homogeneous distribution of the detector material and the lower precision of the measurements, applying the GSF does not result in any appreciable improvements.

Using the GSF, all the tracks with transverse momentum $p_T > 400$ MeV and $|\eta| < 2.5$ that are assigned to electrons [5] in an event can be refitted. The resulting new collection of bremsstrahlung-corrected tracks and the corresponding electromagnetic clusters form new inputs to the standard electron reconstruction algorithm. This procedure has several advantages:

1. The approach described above is expected to improve the estimation of bending-plane quantities, as is presented in more detail in Section 3. In particular, their dependence on the amount of material encountered by (and hence the pseudorapidity of) the electron should be significantly reduced as shown in Fig. 2 in the case of simulated single electrons with transverse momenta between 7-80 GeV.

2. The extrapolation of the tracks and their matching to the electromagnetic calorimeter clusters is performed using the re-estimated track parameters. It is therefore expected that in certain cases the track considered as the best match to the electromagnetic cluster will have changed. Some improvements are also possible in the case of the different electron identification categories. This is particularly likely in the case of the so-called "tight" electrons [4, 5] (which make use of both first and second sampling layer calorimeter information, information from the two silicon detectors
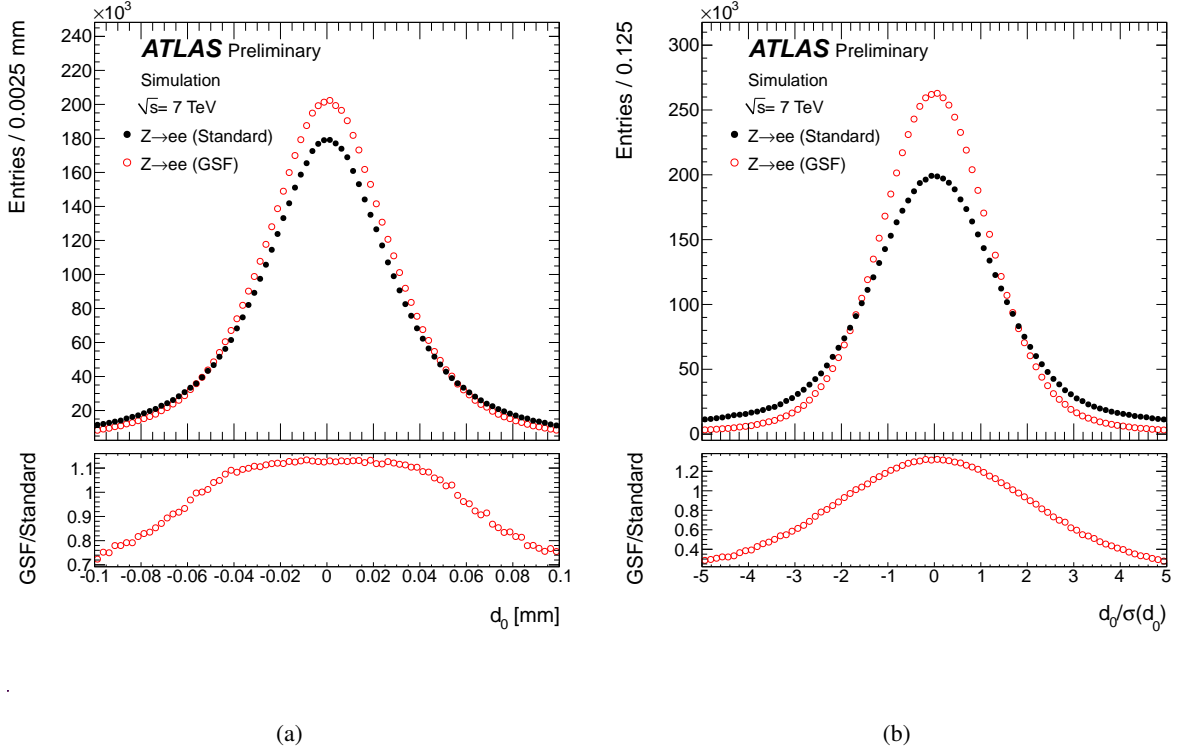
Figure 3: *The distribution of the transverse impact parameter resolution (a) and of the transverse impact parameter significance (b) for both GSF (open red) and standard (solid black) truth-matched Monte-Carlo electrons from Z-boson decays. The bottom plots show the ratio of the entries of the GSF and standard electrons per bin.*

and the Transition Radiation Tracker, E/p, as well as matching between tracking and calorimeter η and ϕ position), where several quantities sensitive to bremsstrahlung losses are employed. The above implications are described in more detail in Section 4.

3. The electron four-momentum is computed using the improved estimates of the track parameters. This is particularly beneficial in the case of low-p_T electrons where the contribution to the resolution of the four-momentum of the track parameters is dominant and where the impact of bremsstrahlung losses is more severe. Furthermore the reconstructed invariant masses of resonances decaying into two electrons are also better evaluated. Both of the above are especially relevant in the case of the J/ψ resonances, where lower energy electrons are involved, as is demonstrated in Section 5.

3 Electron Track Parameters

This section focuses on presenting the improvements in the track parameters in the transverse plane. It should be noted that a full account of the radiative energy losses of an electron is practically impossible. Although the track parameters do improve, some bias will always remain. This is especially the case if the electron has lost significant amounts of energy due to bremsstrahlung at low radius inside the ATLAS Inner Detector, e.g. in the first two Pixel Detector layers. Radiative energy losses are expected to only marginally affect the track parameters in the longitudinal plane. For the results presented in this section when simulated data samples are presented, only reconstructed electrons that pass the "loose++" [4, 5] selection and have been associated to the corresponding generator ones, referred to as truth-matched
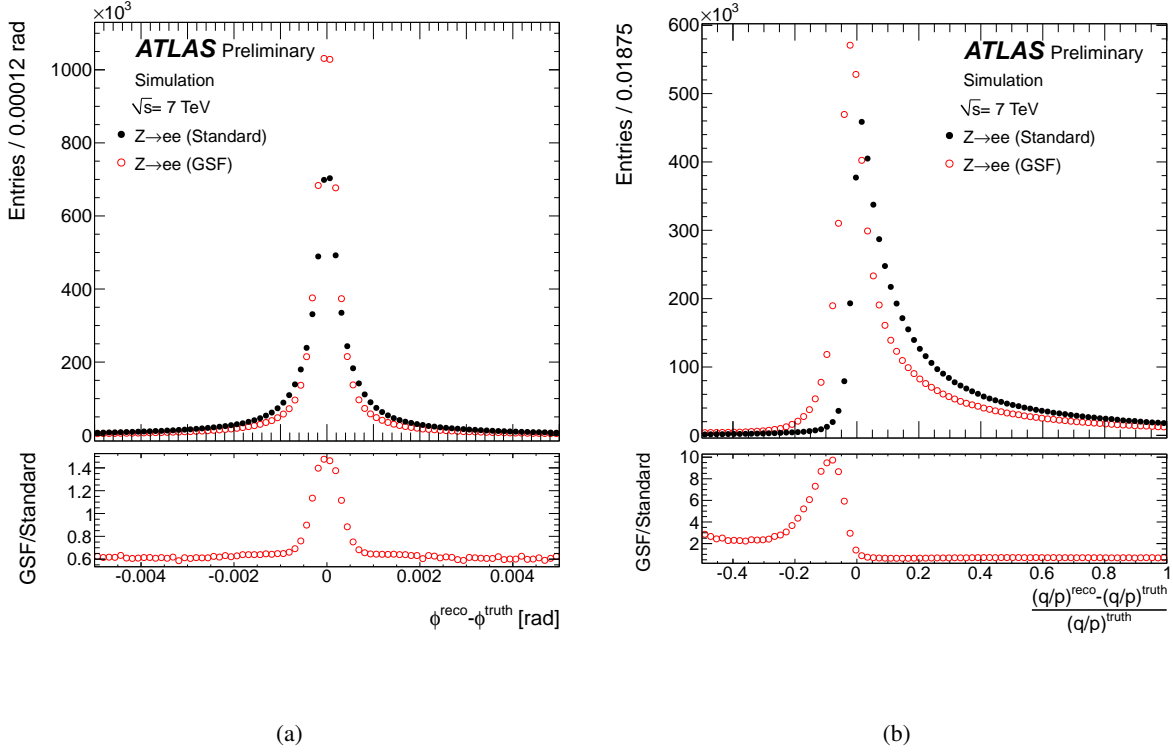
Figure 4: *The distribution of the resolution of the track direction ϕ at the perigee (a) and of the relative bias on the track inverse momentum multiplied by the charge q/p (b), for both GSF (open red) and standard (solid black) truth-matched Monte-Carlo electrons from Z-boson decays. The bottom plots show the ratio of the entries of the GSF and standard electrons per bin.*

Monte-Carlo electrons, are used.

3.1 Transverse Track Parameters Resolution

The distributions of the transverse track parameters are shown in Figs. 3 and 4 for the case of electrons from Z-boson decays. In Fig. 3(a) the resolution of the transverse impact parameter d_0 is shown. The transverse impact parameter significance d_0/σ_{d_0} is defined as the ratio of the transverse impact parameter d_0 to the error from the track fitting procedure, σ_{d_0}, and is shown in Fig. 3(b). Fig. 4(a) shows the resolution of the track direction ϕ at the perigee. Finally, the relative bias of the track inverse momentum multiplied by the charge q/p is shown in Fig. 4(b). As expected, there is a clear improvement in the resolution of all the bending-plane track parameters when radiative losses are accounted for during the track fitting. This could potentially have important implications in physics analyses, for example in the Higgs-boson searches via its decay into two Z-bosons with at least one of the latter subsequently decaying into two electrons. Here, the final-state electrons resulting from the Higgs-boson decay sequence can be separated from those originating from heavy-quark decays by a cut on the transverse impact parameter significance since electrons from heavy quark decay are expected to have large true d_0 values, whereas the true transverse impact parameter of electrons from Z decays should be zero. Equally important is the dependence of the transverse track parameters resolution width (or of the mean relative bias in the case of the track q/p) on the electron pseudorapidity η or transverse momentum p_T as shown in Figs. 5 and 6. At larger pseudorapidities, the amount of material encountered by the electron increases, resulting in increased degradation of the reconstructed track parameters. As is evident in Fig. 5, accounting for the
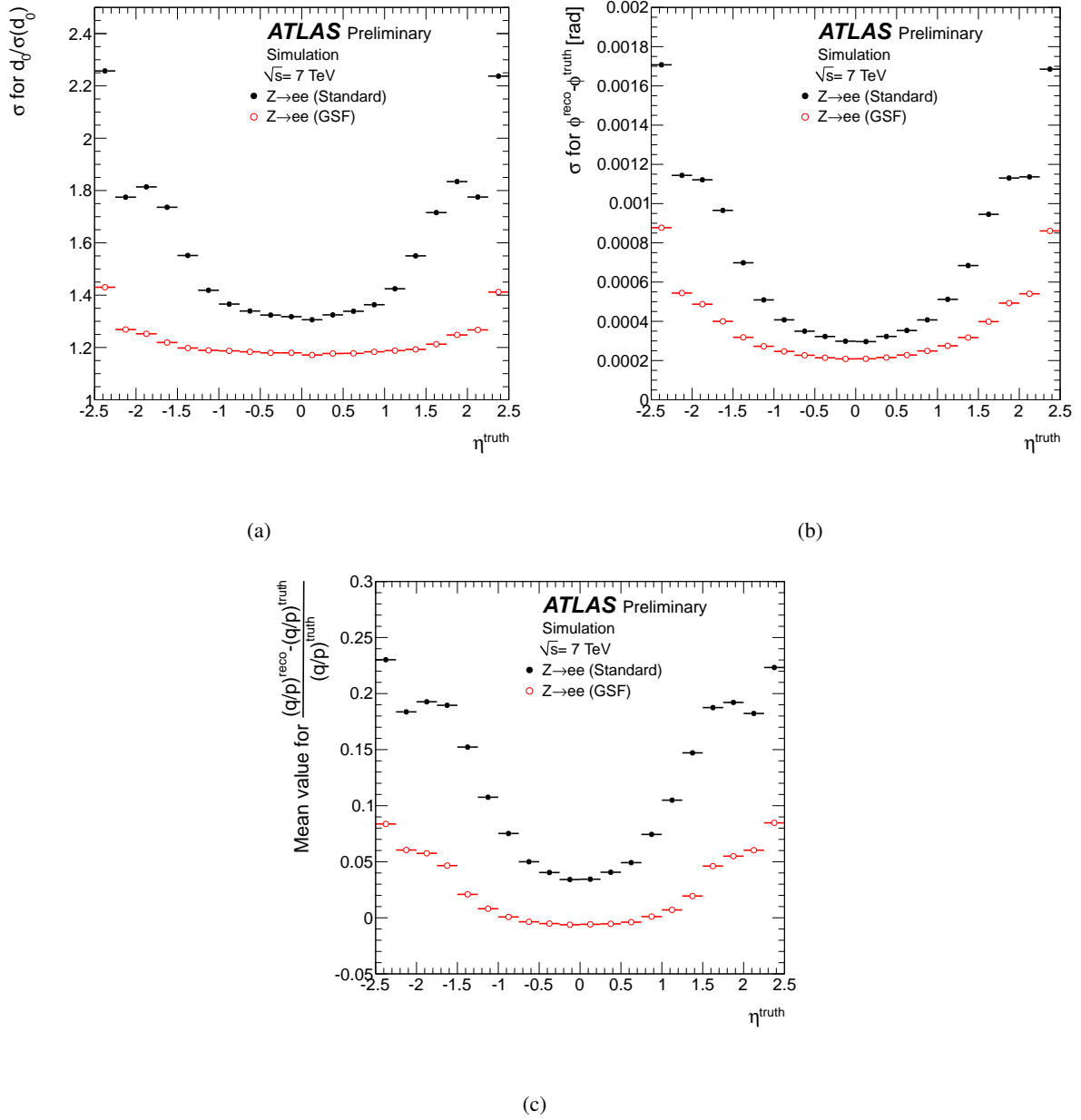
(a)   (b)

(c)

Figure 5: *The dependence on the pseudorapidity η of the width of the transverse impact parameter significance (a), of the width of the resolution of the track direction at the perigee φ (b), and of the mean relative bias of the track inverse momentum multiplied by the charge q/p (c), for GSF (open red) and standard (solid black) truth-matched Monte-Carlo electrons from Z-boson decays.*

bremsstrahlung losses during the track fitting reduces these effects. In addition, the mean relative bias on the reconstructed electron track inverse momentum multiplied by the charge (q/p) is reduced.

3.2   Comparison with Data for the Transverse Impact Parameter Significance

In data, electrons produced by heavy-quark or Z-boson decays can be arranged in two separate samples and then be used to check how well the simulation describes the reconstructed transverse impact parameter significance when the bremsstrahlung corrections are included. Electrons from *b*-hadron decays are
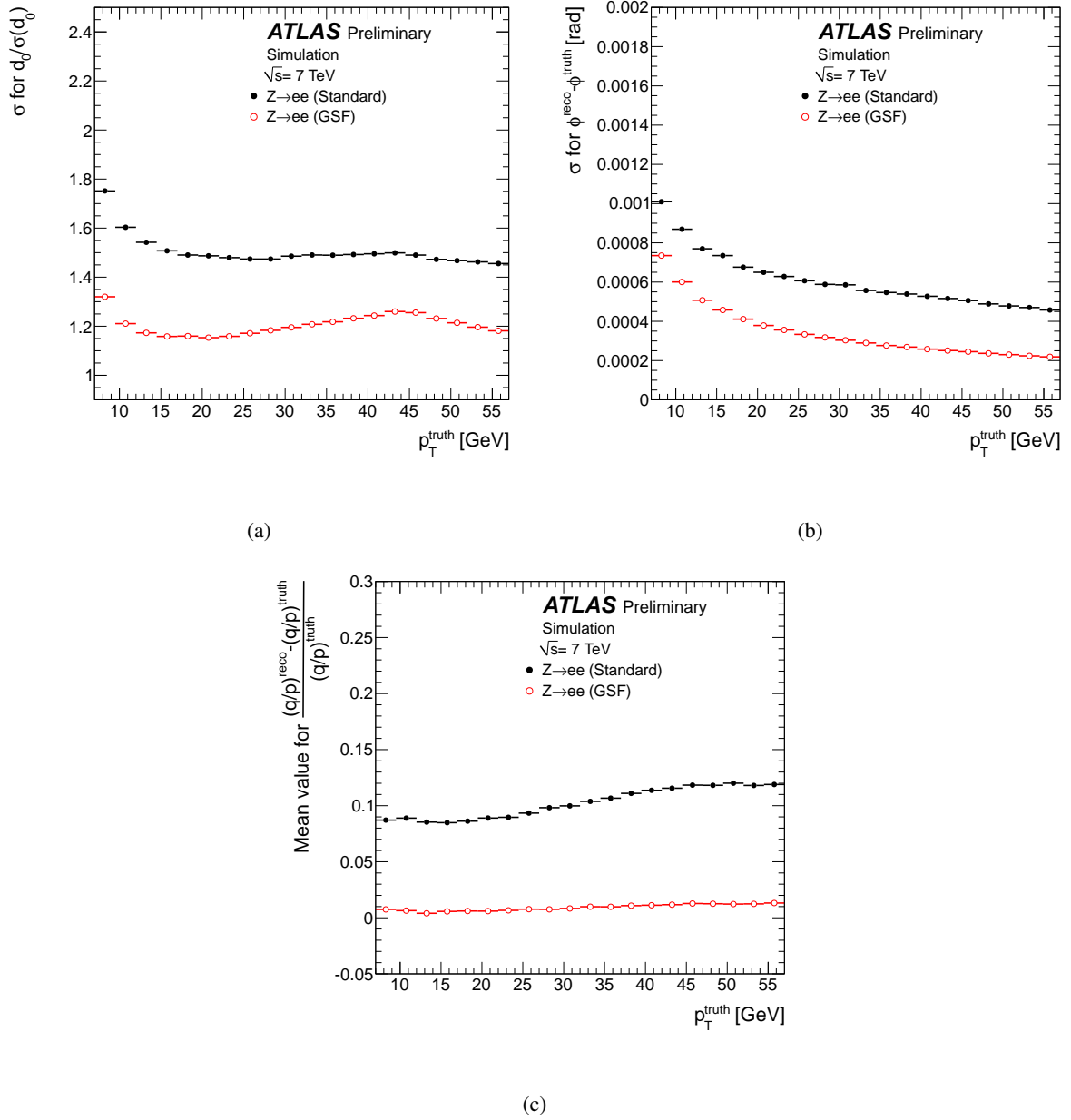
(a)

(b)

(c)

Figure 6: *The dependence on the transverse momentum p_T of the width of the transverse impact parameter significance (a), of the width of the resolution of the track direction at the perigee ϕ (b), and of the mean relative bias of the track inverse momentum multiplied by the charge q/p (c), for GSF (open red) and standard (solid black) truth-matched Monte-Carlo electrons from Z-boson decays.*

selected in data events where either a Z-boson [12] or a $t\bar{t}$ pair (through the dilepton channel [13]) has already been identified. At least one b-tagged jet with $p_T > 25$ GeV is required in the event. One can then look for additional electrons in the selected events that have a well-reconstructed cluster matched to a track, with $p_T > 7$ GeV and $|\eta| < 2.47$ and pass the "loose++" selection criteria. These electrons are required to lie within a cone $\Delta R < 0.5$ around the tagged jet. On the other hand, electrons from Z-boson decays are identified using a tag-and-probe approach. The tag electron is an isolated electron that passes the "tight" selection, while the probe electron is only required to pass the "loose++" selection, using the criteria defined in [4, 5]. The two electrons are required to have opposite charges and to have an invariant
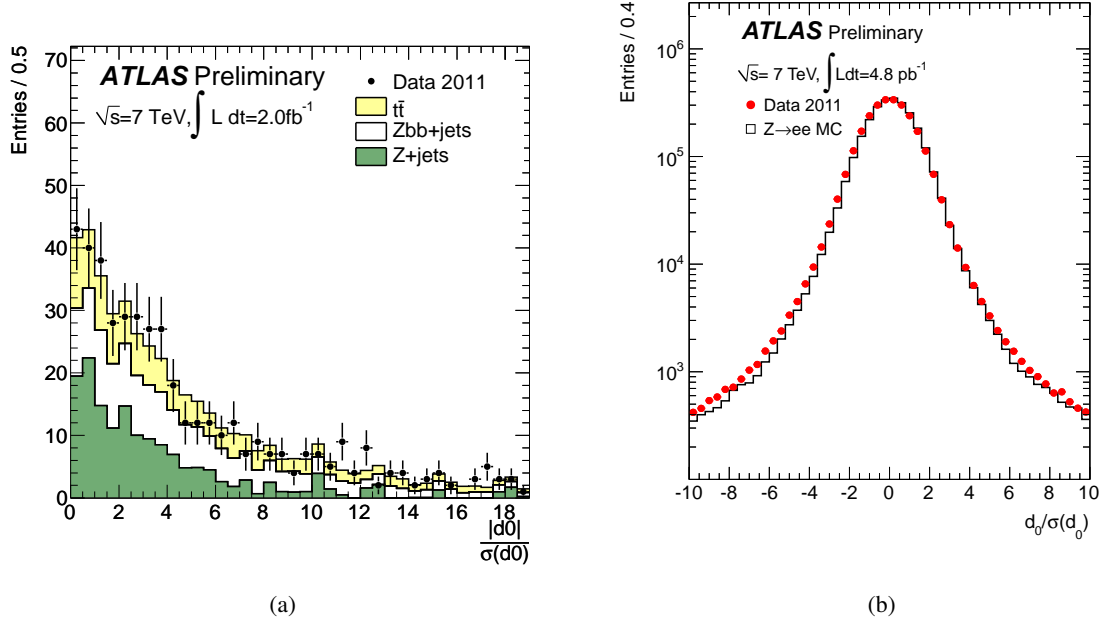
Figure 7: *Comparison between data and simulation of the reconstructed transverse impact parameter significance for GSF-reconstructed electrons from heavy-quark decays (a) (where due to the limited statistics the absolute value of the transverse impact parameter significance is used instead) and from Z-boson decays (b). The small shift visible between the MC and the data distributions in the latter plot is due to a feature in the ATLAS simulation that is unrelated to the bremsstrahlung treatment studied in this note.*

mass within 15 GeV from that of the Z-boson. The distribution of the reconstructed transverse impact parameter significance for electrons refitted using the GSF in data is shown in Fig. 7. The agreement between the data and the simulation is very good.

4 Electron Combined-Parameter Performance

Combined parameters are computed using the selected electron tracks as described in Section 3 and the associated calorimeter information via the track-to-calorimeter matching criteria. The ATLAS Liquid-Argon Electromagnetic Calorimeter extends to a pseudorapidity of $|\eta| = 3.2$. Over the $|\eta| < 2.5$ range covered by the tracker, it makes precision measurements with three sampling depths. The combined parameters discussed in this section include the calorimeter energy to track momentum ratio (E/p), and the difference in the extrapolated track impact point to the second sampling of the calorimeter ϕ cluster barycentre position ($\Delta\phi_2$). The latter has been multiplied by the charge sign so that the impact point difference is independent of the particle charge. They are used in the electron identification algorithms, particularly in the so-called "tight++" identification [4, 5], which makes use of both first and second sampling layer calorimeter information, information from the two silicon detectors and the Transition Radiation Tracker, E/p, as well as matching between tracking and calorimeter η and ϕ position.

The following subsections show comparisons of the GSF-refitted simulated electrons to the standard-reconstructed electrons as well as comparisons between simulation and collision data of GSF-refitted electrons from Z-boson decays. One example is also shown for prompt $J/\psi \rightarrow ee$ data, to illustrate the good data to Monte Carlo agreement of GSF electrons at lower energies.
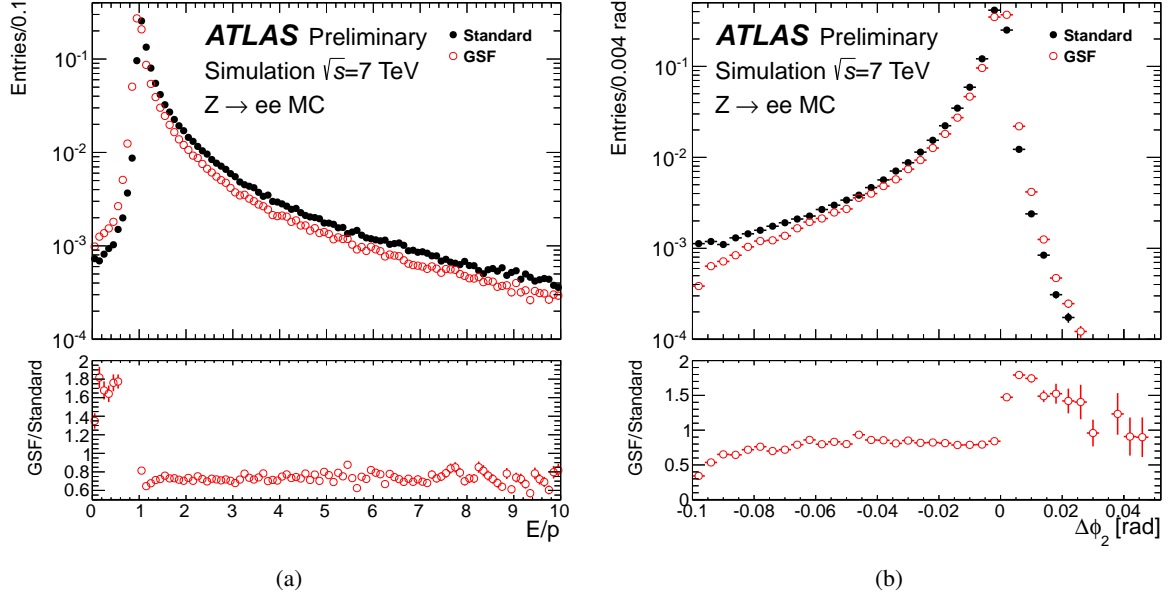
Figure 8: *The distributions of the calorimeter energy to track momentum ratio (E/p in (a)) and of the azimuthal φ difference between the extrapolated track and the corresponding cluster position as measured in the second sampling of the calorimeter (Δφ₂ in (b)), for truth-matched Monte-Carlo GSF (open red) and standard (solid black) electrons. The GSF-to-standard ratio is given below.*

4.1 Combined Track-Calorimeter Parameters

Distributions of E/p and $\Delta\phi_2$ for truth-matched simulated electrons from Z decays are shown in Fig. 8, as well as the dependence of their means on η in Fig. 9. The GSF-refitted electrons are better centred at $E/p = 1$ and $\Delta\phi_2 = 0$ with smaller radiative tails than the standard electrons candidates. The η dependence of the mean of the distributions is noticeably flattened, implying lesser sensitivity to material effects in the case of the GSF-refitted electrons. Figure 10 illustrates the good agreement between data and simulation for the E/p variable for the case of reconstructed electrons in the electromagnetic calorimeter outer barrel ($0.8 < |\eta| < 1.37$). Figure 11 shows an equivalent plot for $J/\psi \to ee$ events which represent electrons with fairly low energies in the range 7 GeV$< E_T <$15 GeV where, as discussed earlier in this note, radiative energy losses are more pronounced.

4.2 Electron Identification Efficiencies

Since the GSF-refitted tracks and their associated calorimeter cluster information form the new input to the electron identification algorithm, electron identification efficiencies are expected to improve. The "tight++" electron identification efficiency with respect to Monte-Carlo truth information is shown in Fig. 12 as a function of electron η. Electrons refitted with GSF show an improvement in the electron identification efficiency of over 5% at high $|\eta|$. The improvement as a function of transverse momentum is approximately 2% at 15 GeV and 0.5% at 70 GeV. The "tight++" selection requirements used in the plots shown have been optimised for the older standard electrons. Further improvement might be achieved by reoptimising these requirements when the new GSF-refitted tracks are used.
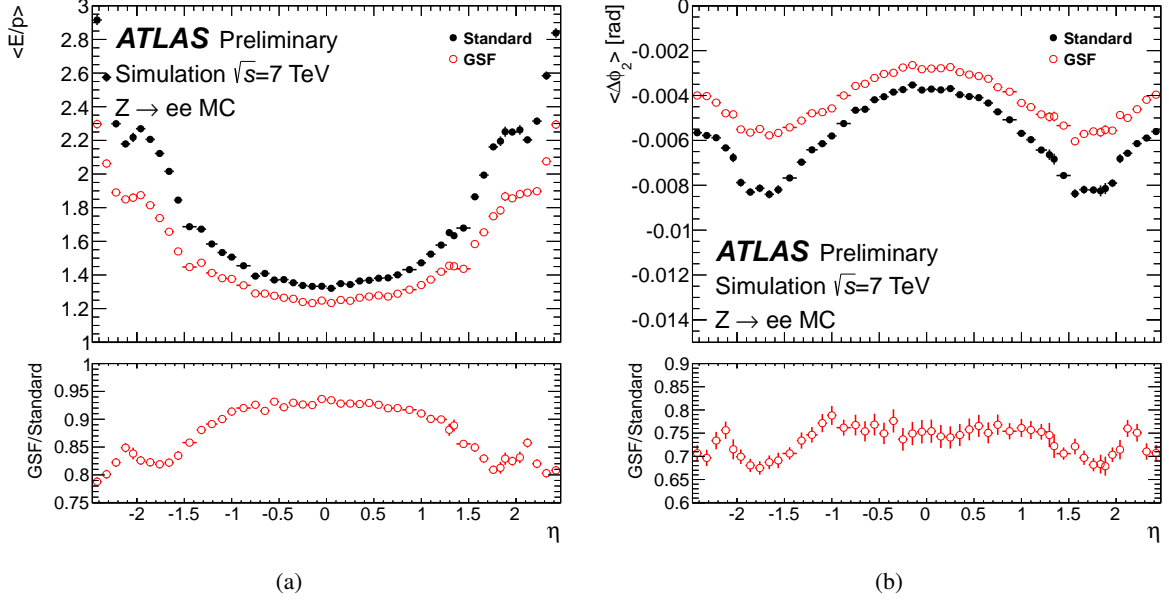
9

Figure 9: *The dependence on the pseudorapidity η of the mean calorimeter energy to track momentum ratio (E/p, in (a)) and of the mean difference of extrapolated track φ to the cluster φ position as measured in the second sampling of the calorimeter (Δφ₂ in (b)), for truth-matched Monte-Carlo GSF (open red) and standard (solid black) electrons. The GSF-to-standard ratio is given below.*

4.3 Choice of Tracks Matched to Clusters

It is instructive to see how often a different track is matched to the calorimeter cluster as a result of the GSF-refitting, compared to the standard tracking. This information is shown in Fig. 13 as a function of η. In the central η region, a new track is rarely selected, but this choice is changed in approximately 5% of the cases at high $|\eta|$. Matching to different tracks is largely independent of p_T, averaging approximately 0.8% over the entire p_T kinematic range.

5 J/ψ Invariant Mass Shape with GSF-refitted Electrons

The greatest improvements in electron reconstruction after implementing bremsstrahlung correction techniques are expected at low ($\lesssim 15$ GeV) transverse energies. The J/ψ meson ($m_{J/\psi} = 3069.9$ MeV [14]) provides an abundant source of low energy di-electron final states, and is therefore a testbed tool for validation studies of these bremsstrahlung-aware reconstruction tools. In addition to an increase in the reconstruction and identification efficiencies, gains in the resolution of electron kinematic quantities will lead to improvements in the accuracy of the parent J/ψ four-vector. As a result, the position of the peak of the parent invariant mass distribution should be more accurate, which could be important in the measurement of the mass of new particles (e.g. exotic new quarkonia states). The mass resolution is also expected to improve, which is particularly desirable for the separation of closely spaced states such as the $\Upsilon(1S)$, $\Upsilon(2S)$ and $\Upsilon(3S)$. Other indirect benefits may also be seen in physics measurements that are reliant on angular distributions (e.g. polarisation), or those which are sensitive to bin migrations (such as differential cross-sections). Aside from the best-fit values for the kinematic variables, an improvement is also expected in the covariance matrix for the four-vectors benefiting, for example, the vertex position fits and lifetime measurements.
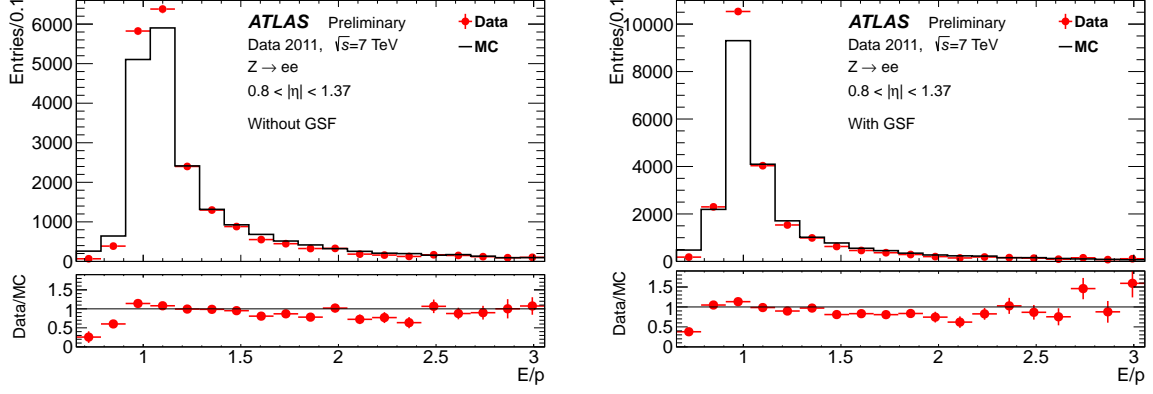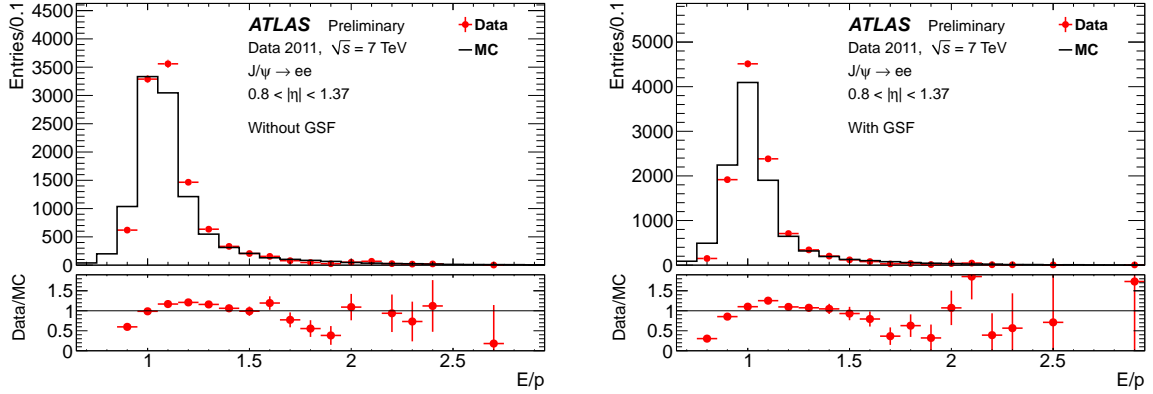
Figure 10: *Comparison of the data to a simulation of the calorimeter energy to track momentum ratio (E/p), for 0.8 < |η| < 1.37 using standard (left plot) and GSF (right plot) tracking for Z → ee candidate electrons with reconstructed electron energy 15 GeV< E_T <25 GeV.*

Figure 11: *Comparison of the data to a simulation of the calorimeter energy to track momentum ratio (E/p), for 0.8 < |η| < 1.37 using standard (left plot) and GSF (right plot) tracking for J/ψ → ee candidate electrons with reconstructed electron energy 7 GeV< E_T <15 GeV.*

5.1 J/ψ Candidate Selection

This study uses a Monte-Carlo data sample of about 5 million prompt J/ψ produced by the PYTHIA 6 [15] generator (which uses the MRST LO* [16] parton distribution functions) with an ATLAS-specific tune [17]. *Prompt* refers to those J/ψ directly produced in the primary (hard) interaction, or from the decay of excited charmonium states (e.g. $\chi_{c1} \to \gamma J/\psi$). A non-prompt J/ψ sample was also initially studied, but showed similar results to the prompt sample and so is not discussed here. A subset of the full 2011 collision data-set (approximately 37 million events recorded early during the data-taking campaign and combining all contributing electron triggers) is also included in the analysis for comparison with the simulation. For both the data and simulation samples, events were processed with (1) the standard electron reconstruction algorithm and (2) the modified algorithm where the GSF is used to refit all tracks associated to each electromagnetic cluster, leaving the track-cluster matching and identification criteria unchanged.

A standard candidate selection is employed, which requires two opposite-sign reconstructed electrons, each with an associated track containing at least 6 silicon hits (with at least one of these in the
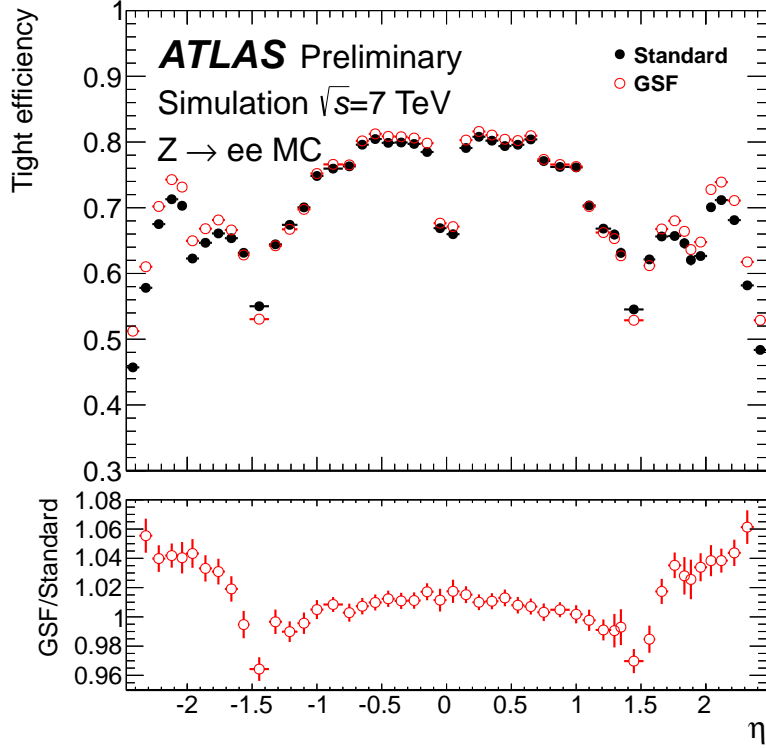
11

Figure 12: *The "tight++" electron identification efficiency with respect to Monte-Carlo truth as a function of η , for GSF (open red) and standard (solid black) electrons. The GSF-to-standard ratio is given below.*

pixel detector). Both electrons are required to fulfil the "tight" electron identification criteria. For each $J/\psi \to ee$ decay candidate passing these selections, the two electron tracks are then fitted to a common vertex with the requirement on the fit quality that $\chi^2_{\text{vertexfit}} < 200$. Precise knowledge of the position of the vertex is essential in any attempt to separate prompt from non-prompt J/ψ. The resulting vertex-refitted tracks and their corresponding covariance matrices are then used to construct the J/ψ four-vector and covariance matrix, from which the invariant mass and uncertainty ($m_{e^+e^-}$ and $\delta m_{e^+e^-}$, respectively) are calculated.

5.2   Results and Discussion

The invariant mass distributions for the prompt simulation sample are shown in Fig. 14(a), with the results for the standard electron reconstruction and reconstruction using GSF track fitting, normalized to the same number of entries, overlaid for comparison. The shape of the curve for the GSF-refitted electrons is much more symmetrical about its peak value, which is in addition closer to the PDG value of 3096.9 MeV [14]. A tail to the left of the peak remains due to the inability of the GSF algorithm to account for bremsstrahlung losses when the photon emission occurs very close to the electron production vertex, but as can be seen in the figure, the resolution is indeed narrower when using GSF refitting. These trends are also reflected in the results for the collision data sample (Fig. 14(b)). The distribution for the data also includes a secondary, smaller peak at the $\psi(2S)$ mass, which is slightly more visible for the GSF reconstruction.

The evolution of the mass shape with the pseudorapidity of the electrons is another point of interest. In Fig. 15(b), the invariant mass for the GSF-refitted Monte-Carlo J/ψ sample is displayed as a function
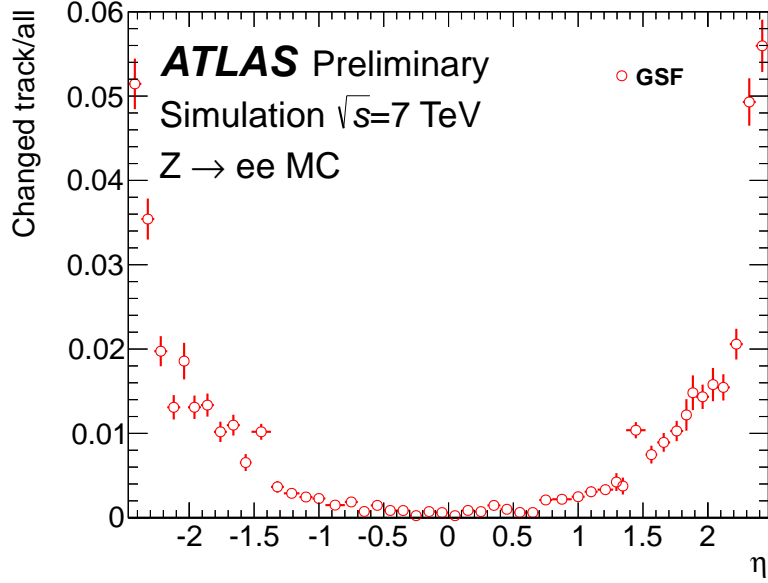
Figure 13: *Fraction of Monte-Carlo electron candidates for which a different track was matched to the calorimeter cluster as a result of GSF-refitting (compared to the original track selection for standard tracking) as a function of η.*

of the parent J/ψ rapidity. The width of the distributions is strongly dependent on the rapidity, but the position of the peak is more stable than in the case of the standard electron reconstruction (Fig. 15(a)). The observed poorer resolution in the forward regions is as expected, since for these trajectories there is generally more material in the detector and less coverage by the tracking elements.

To quantify the shapes of the GSF distributions, binned maximum-likelihood fits were performed using the Crystal Ball (CB) function for the signal peak and a second order Chebychev polynomial to describe the background. The intrinsic width of the mass distributions is a function of the rapidity (see Fig. 15(b)). An accurate description of the signal shape across the entire rapidity range would require several CB curves to account for this. This complication was avoided by restricting the rapidity range of the J/ψ candidates to $|y| < 0.1$, where the width is essentially constant. For the collision data sample, a second CB was used to describe the $\psi(2S)$ resonance. The fits for the two samples are given in Fig. 16, with values for the peak parameter $m_{J/\psi}$ of 3105–3107 MeV, and having consistent widths. Though the position of the mean is slightly above the PDG value (by approximately 10 MeV), it is a clear improvement over the peak value for standard electron reconstruction, which is at approximately 3020 MeV. The widths measured in these fits using the GSF algorithm (73 and 85 MeV for simulation and data, respectively) are much narrower compared to the results when using calorimeter measurements of transverse energy on similar data samples (typically $\gtrsim$ 110 MeV). For comparison, distributions for $J/\psi \rightarrow \mu^+\mu^-$ decays are symmetric and have a width of about 50 MeV [18]. The success of the CB fits here in describing the peak shape is encouraging, as it is important for accurate extraction of yields for cross-section measurements.
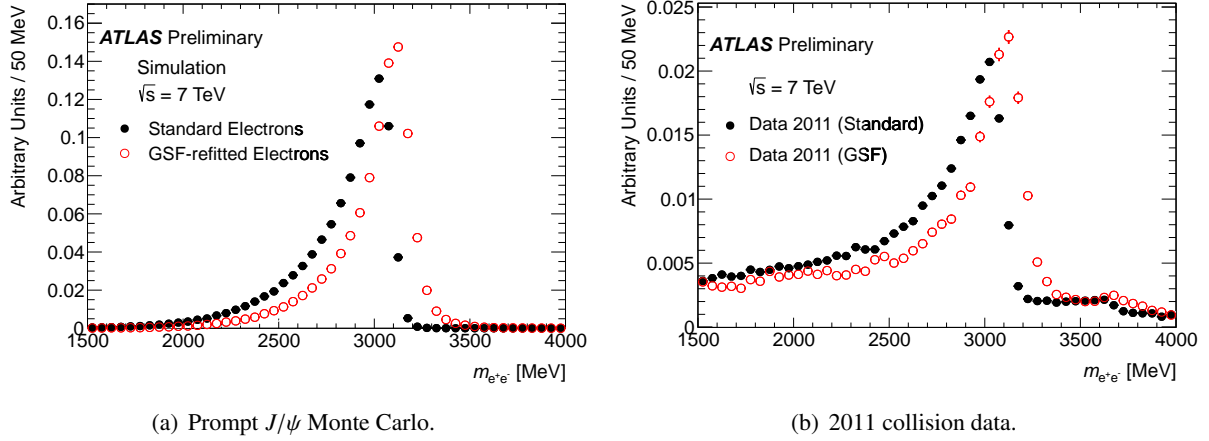
(a) Prompt J/ψ Monte Carlo.

(b) 2011 collision data.

Figure 14: *The e^+e^- invariant mass distributions for prompt J/ψ simulation (a) and 2011 collision data samples (b).*

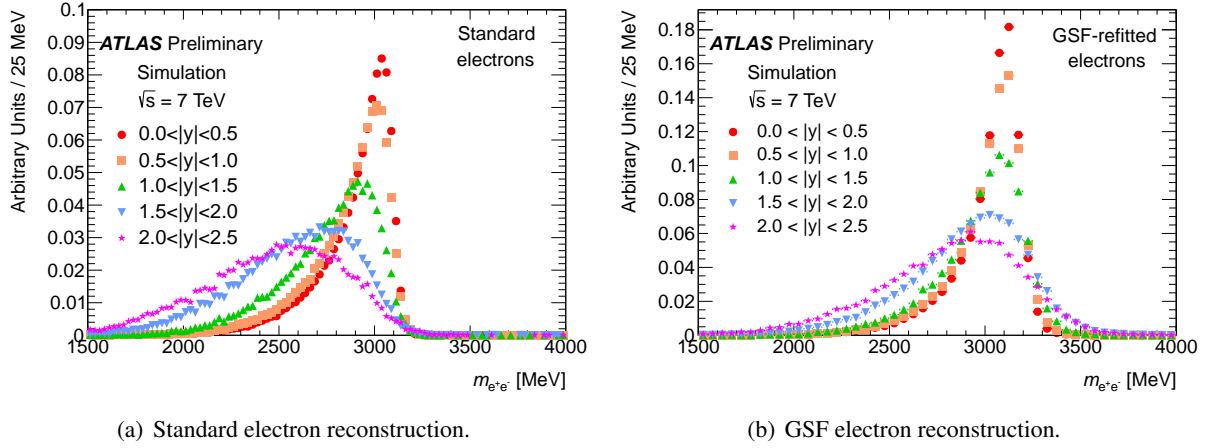(a) Standard electron reconstruction.

(b) GSF electron reconstruction.

Figure 15: *The invariant mass distributions as a function of the combined e^+e^- rapidity for the standard (a) and GSF reconstruction (b) of simulated J/ψ decays. While the widths of the distributions clearly increase in the more forward η regions, the GSF algorithm successfully stabilises the position of the peak.*

6   Summary and Conclusions

A modification of the ATLAS electron reconstruction scheme, that uses track refitting with the Gaussian Sum Filter (GSF) algorithm to account for the effects of bremsstrahlung, is presented in this note. It is demonstrated that this procedure leads to an improved estimation of bending-plane quantities such as the transverse impact parameter significance, track angular direction at the perigee ϕ, and the inverse momentum multiplied by the charge q/p. Distributions of combined track and calorimeter parameters such as the calorimeter energy to track momentum ratio, E/p, as well as the difference in extrapolated track impact point to the calorimeter second sampling ϕ cluster barycentre position, $\Delta\phi_2$, are observed to be narrower and less dependent on the amount of material traversed by the electron, which is a function of the electron pseudorapidity, being larger at large $|\eta|$. Improvements on the order of up to 5% for electron identification efficiency at large $|\eta|$ in the endcap regions are also demonstrated. Significant improvements are observed in the invariant mass mean and width of $J/\psi \to ee$ since the electron four-momentum is computed using the better-estimated track parameters. This note concludes the first phase of a two-step programme in ATLAS to improve the electron reconstruction aiming at correcting all tracks
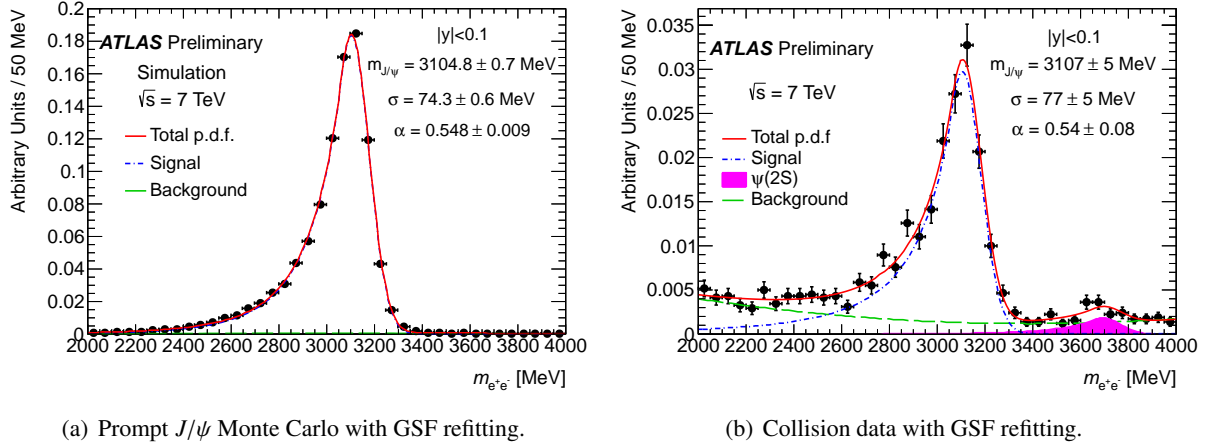
(a) Prompt J/ψ Monte Carlo with GSF refitting.

(b) Collision data with GSF refitting.

Figure 16: *The mass distributions for the GSF-refitted prompt J/ψ Monte Carlo (a) and collision data samples (b) restricted to a rapidity range $|y| < 0.1$ and fitted using a single Crystal Ball function for the signal (dashed blue line) and a second order Chebyshev polynomial (dashed green line) for the background. In the case of the real data, a second CB function was required to account for the $\psi(2S)$ (purple filled area). The overall fit is shown in red. The resulting Crystal Ball fit parameters, $m_{J/\psi}$, σ and α, are displayed with their uncertainties on the plot.*

associated to electron candidates by performing bremsstrahlung *refitting* prior to electron reconstruction and identification. It will be followed by a bremsstrahlung *recovery* at the initial step of reconstruction, making it the new default electron reconstruction scheme in ATLAS.

References

[1] ATLAS Collaboration, G. Aad et al., *The ATLAS Experiment at the CERN Large Hadron Collider*, JINST **3** (2008) S08003.

[2] R. Fruehwirth, *A Gaussian-mixture approximation of the Bethe-Heitler model of electron energy loss by bremsstrahlung*, Comp. Phys. Comm. **154** (2003) 131.

[3] T. M. Atkinson. PhD thesis, The University of Melbourne, 2006.

[4] ATLAS Collaboration, *Electron performance measurements with the ATLAS detector using the 2010 LHC proton-proton collision data*, Eur. Phys. J. **C72** (2012) 1909.

[5] ATLAS Collaboration, *Expected electron performance in the ATLAS experiment*, ATLAS-PHYS-PUB-2011-006 (2011) .

[6] ATLAS Collaboration, T. Cornelissen et al., *Concepts, Design and Implementation of the ATLAS New Tracking (NEWT)*, ATLAS-SOFT-PUB-2007-007 (2007) .

[7] ATLAS Collaboration, *Expected Performance of the ATLAS Experiment - Detector, Trigger and Physics*, arXiv:0901.0512 [physics.hep-ex].

[8] H. Bethe and W. Heitler, *The Quantum Theory of Radiation*, Proc. R. Soc. **A146** (1934) 83.

[9] A. Schaelicke et al., *Improved Description of Bremsstrahlung for High-Energy Electrons in Geant4*, IEEE Nucl. Sci. Symp. Conf. Rec. **N37-1** (2008) 2788.

[10] The GEANT4 Collaboration, S. Agostinelli et al., *GEANT4: A simulation toolkit*, Nucl. Instrum. Meth. **A506** (2003) 250.

[11] R. Fruehwirth, *Application of Kalman filtering to track and vertex fitting*, Nucl. Instrum. Meth. **A262** (1987) 444.

[12] ATLAS Collaboration, *Measurement of the cross-section for b-jets produced in association with a Z-boson at $\sqrt{s}$ = 7 TeV with the ATLAS detector*, Phys. Lett. B **706** (2012) 295.

[13] ATLAS Collaboration, *Measurement of the top quark pair production cross section in pp collisions at $\sqrt{s}$ = 7 TeV in dilepton final states with ATLAS*, ATLAS-CONF-2011-100 (2011) .

[14] K. Nakamura et al., *Review of Particle Physics*, Physical Review G **37** (2010) 075021.

[15] T. Sjostrand, S. Mrenna, and P. Z. Skands, *PYTHIA 6.4 Physics and Manual*, JHEP **0605** (2006) 026.

[16] A. Sherstnev and R. S. Thorne, *Parton Distributions for LO Generators*, EPJC **55** (2008) 553.

[17] ATLAS Collaboration, *ATLAS tunes of PYTHIA6 and Pythia 8 for MC11*, ATLAS-PHYS-PUB-2011-009 (2011) .

[18] ATLAS Collaboration, *Measurement of the differential cross-sections of inclusive, prompt and non-prompt J/ψ production in proton-proton collisions at $\sqrt{s}$ = 7 TeV*, Nuclear Physics B **850** (2011) no. 3, 387 – 444.
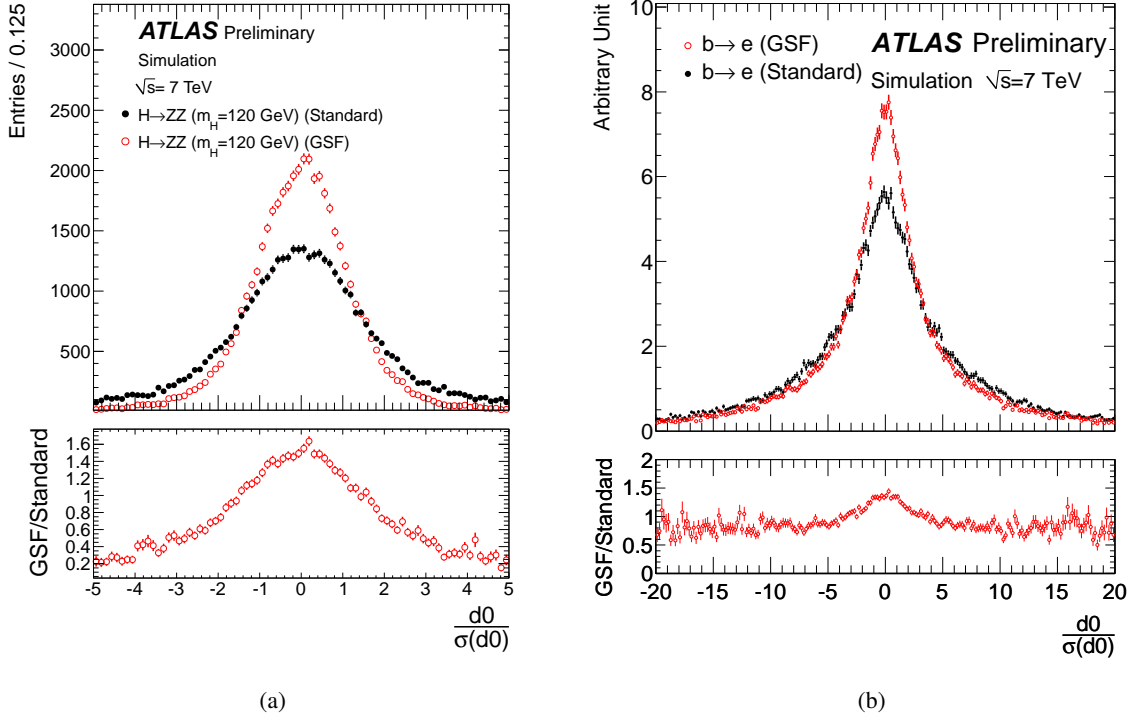
A   Additional Distributions

(a)

(b)

Figure 17: *Truth-matched Monte Carlo distribution of the transverse impact parameter significance for both GSF and standard reconstructed electrons from 120 GeV Standard Model Higgs-boson decays (a) and heavy-quark (b) decays. The bottom plots shows the ratio of the entries of the GSF and standard electrons per bin of d_0/σ_{d_0}.*
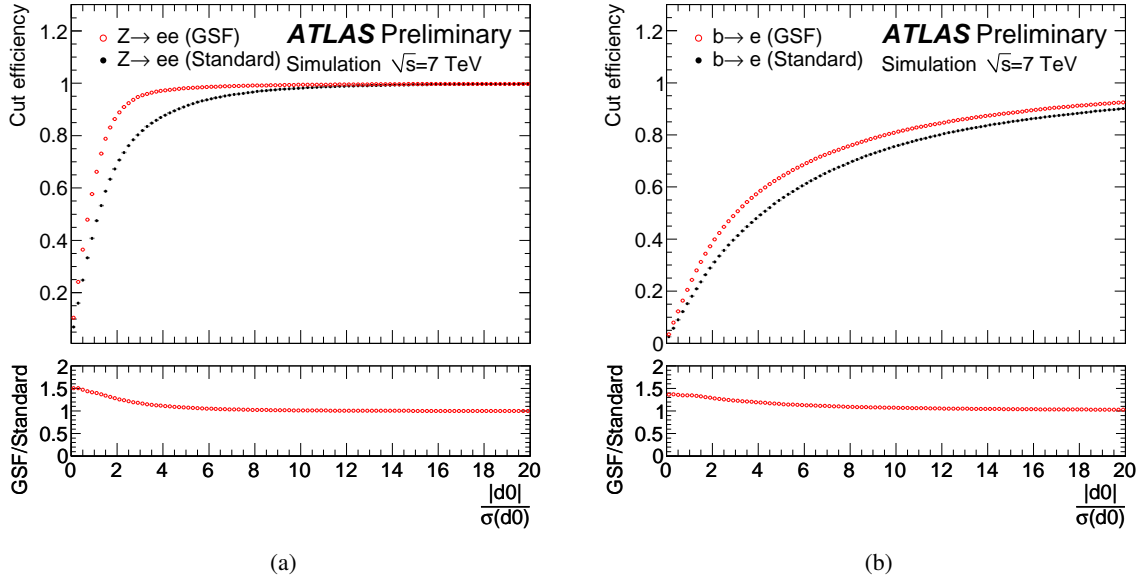

(a)

(b)

Figure 18: *Efficiency for selecting electrons from simulated Z-boson (a) and heavy-quark (b) decays as a function of different requirements on the absolute value of the transverse impact parameter significance.*
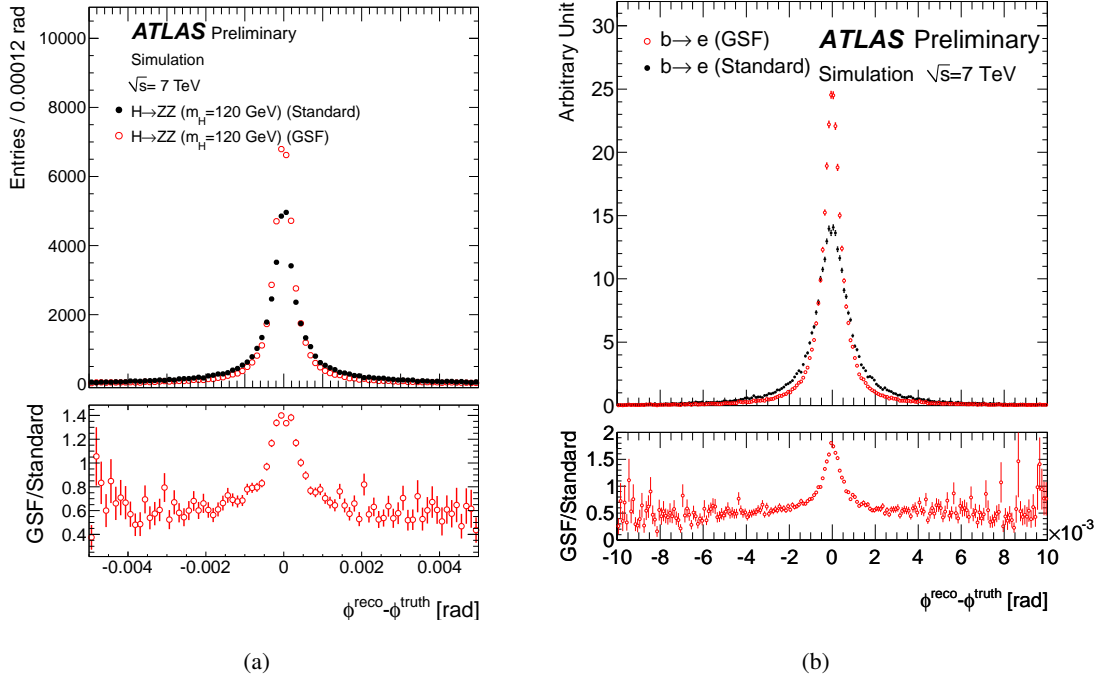
Figure 19: *The resolution of the reconstructed electron track direction angle φ at the perigee for GSF (open red) and standard (solid black) reconstructed simulated electrons from 120 GeV Standard Model Higgs-boson (a) and from heavy-quark decays (b). The bottom plots shows the ratio of the entries of the GSF and standard electrons.*
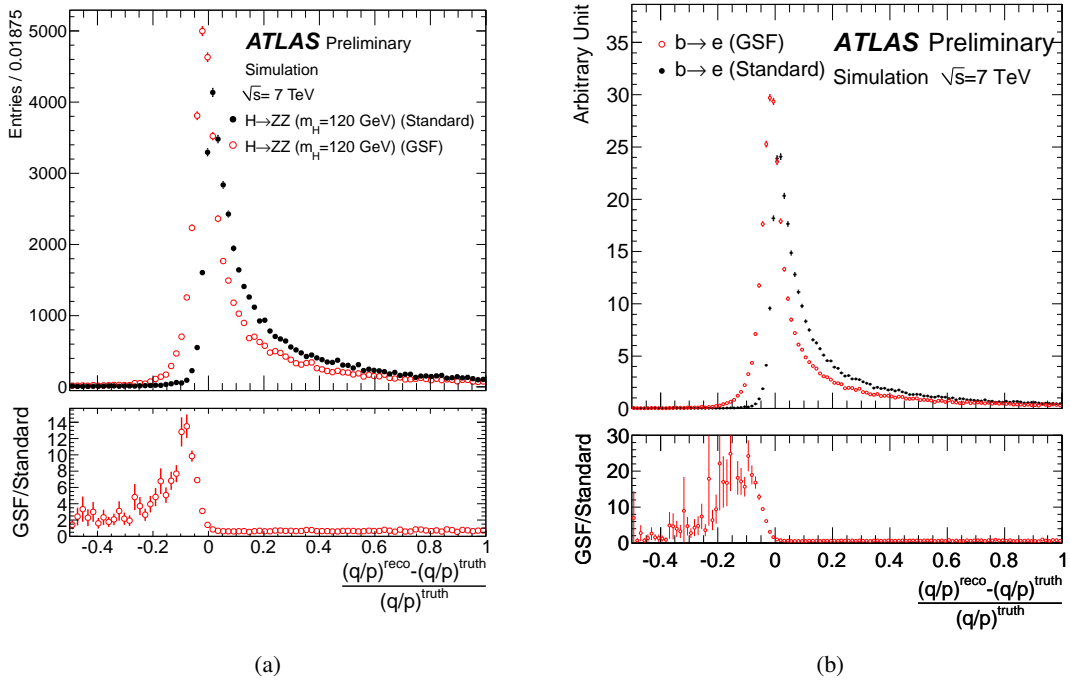

Figure 20: *The relative bias of the reconstructed electron track inverse momentum $1/p$ at the perigee multiplied by the charge q for both GSF (open red) and standard (solid black) reconstructed simulated electrons from 120 GeV Standard Model Higgs-boson decays (a) and from heavy-quark decays (b). In each case the bottom plot shows the ratio of the entries of the GSF and standard electrons per bin of the relative q/p bias.*
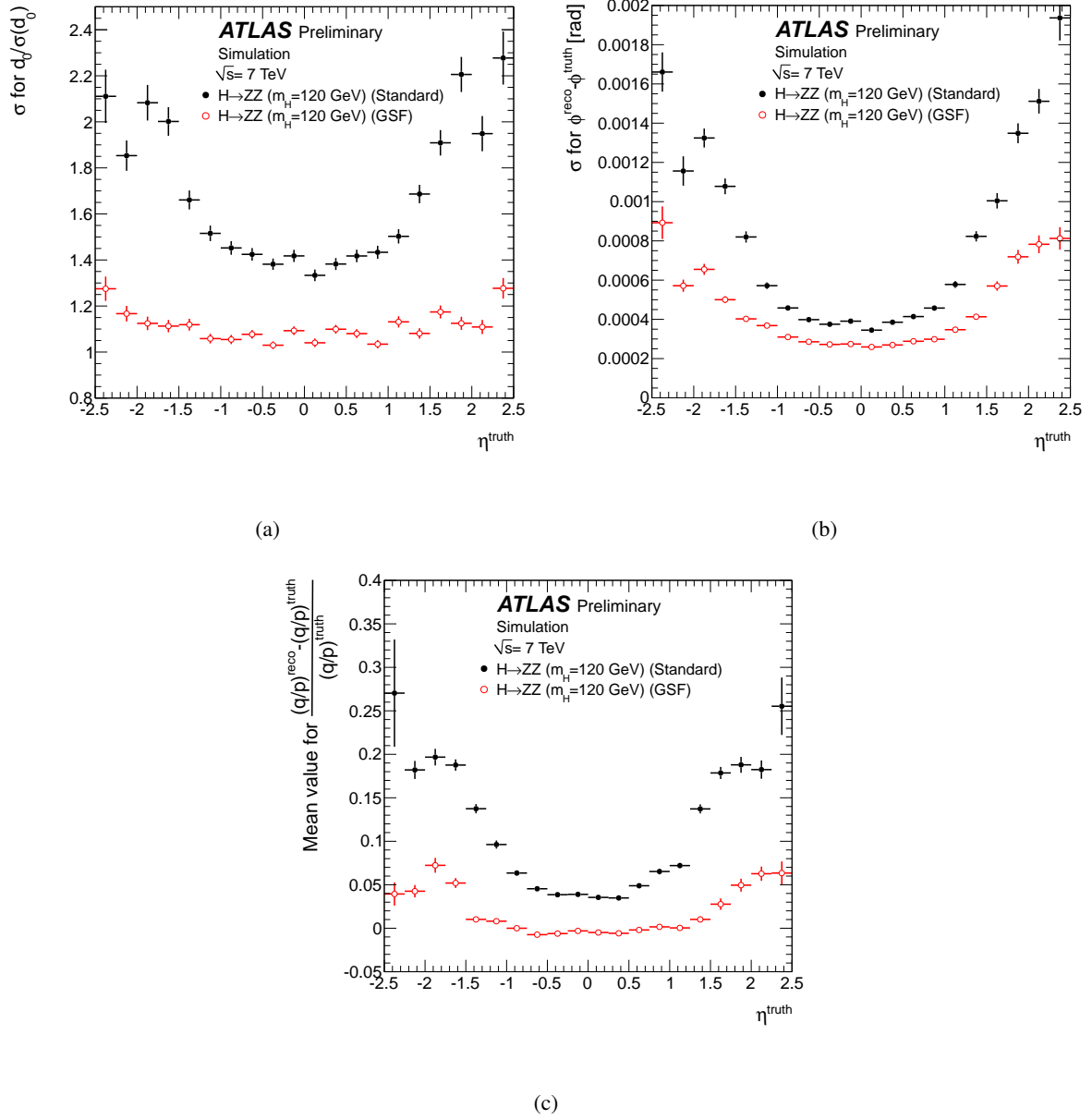
(a)

(b)

(c)

Figure 21: *The transverse impact parameter significance pull width (a), the resolution width of the track direction angle ϕ at the perigee (b) and the mean relative bias of the inverse track momentum multiplied by the charge q/p (c), for truth-matched Monte Carlo electrons as a function of the pseudorapidity η for both GSF (open red) and standard (solid black) reconstructed electrons from 120 GeV Standard Model Higgs-boson decays.*
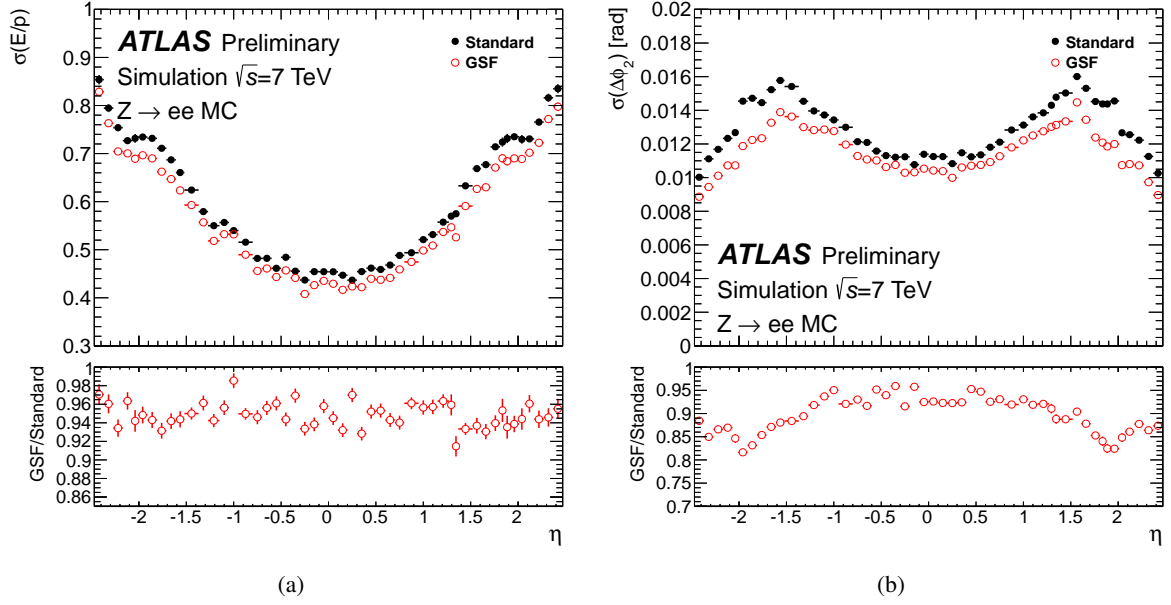
Figure 22: *Truth-matched Monte-Carlo distributions of the width (σ) of the calorimeter energy to track momentum ratio (E/p) (a) and of the mean difference of extrapolated track ϕ to the cluster ϕ position as measured in the second sampling of the calorimeter ($\Delta\phi_2$) (b) as a function of η, for GSF (open red) and for standard (solid black) electrons. The GSF-to-standard ratio is given below.*
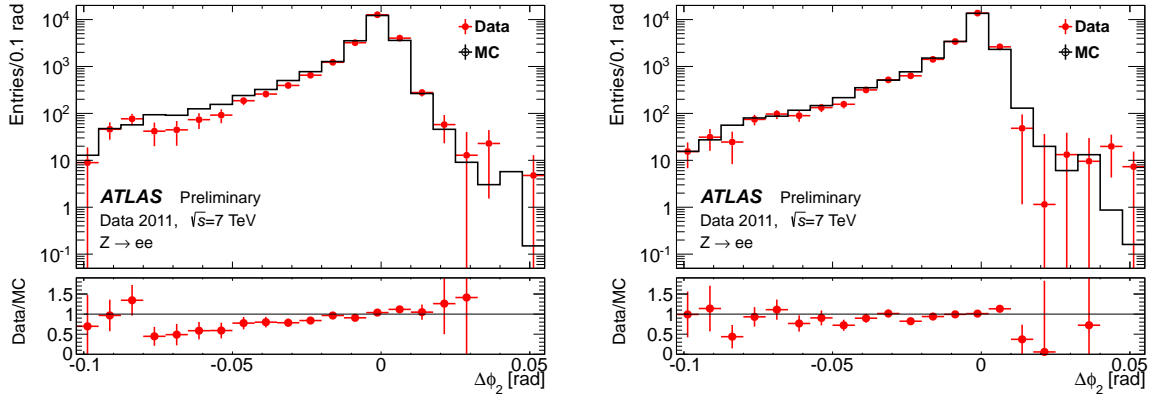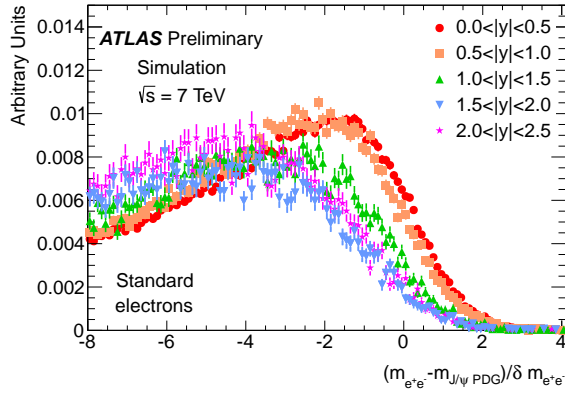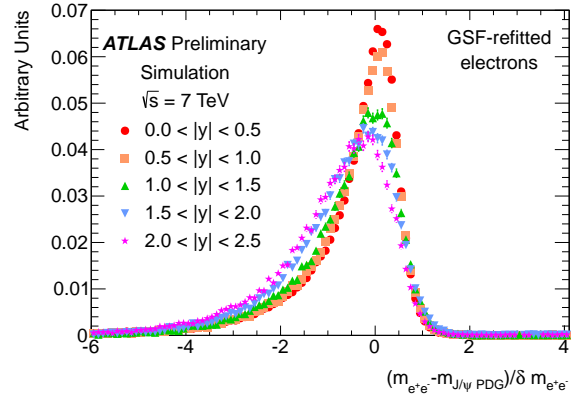

Figure 23: *Data comparison to simulation of the extrapolated track ϕ to the cluster ϕ position as measured in the second sampling of the calorimeter ($\Delta\phi_2$), for $0.8 < |\eta| < 1.37$ (left plot) and $1.52 < |\eta| < 2.0$ (right plot) for $Z \to ee$ candidate GSF electrons with reconstructed electron energy $15\ GeV < E_T < 25\ GeV$.*

20

(a) Standard reconstruction.

(b) GSF reconstruction.

Figure 24: *The pull distribution of the di-electron invariant mass, for the standard (a) and GSF (b) reconstruction of MC electrons from J/ψ decays as a function of the candidate J/ψ rapidity. Ideally, the distributions should be a Gaussian function centered at zero with unity width in the core, though a tail on the negative side is expected. The results for the GSF are less dependent on rapidity and far closer to the desired distribution than those for the standard reconstruction.*